Supplement of

Tree-ring oxygen isotope based inferences on winter and summer moisture dynamics over the glacier valleys of Central Himalaya

Nilendu Singh et al.

Correspondence to: Santosh K. Rai (*rksant@gmail.com*)

This supplementary material consists of 8 Figures and 3 Tables (all referred in the main text)

Supplementary Figures:

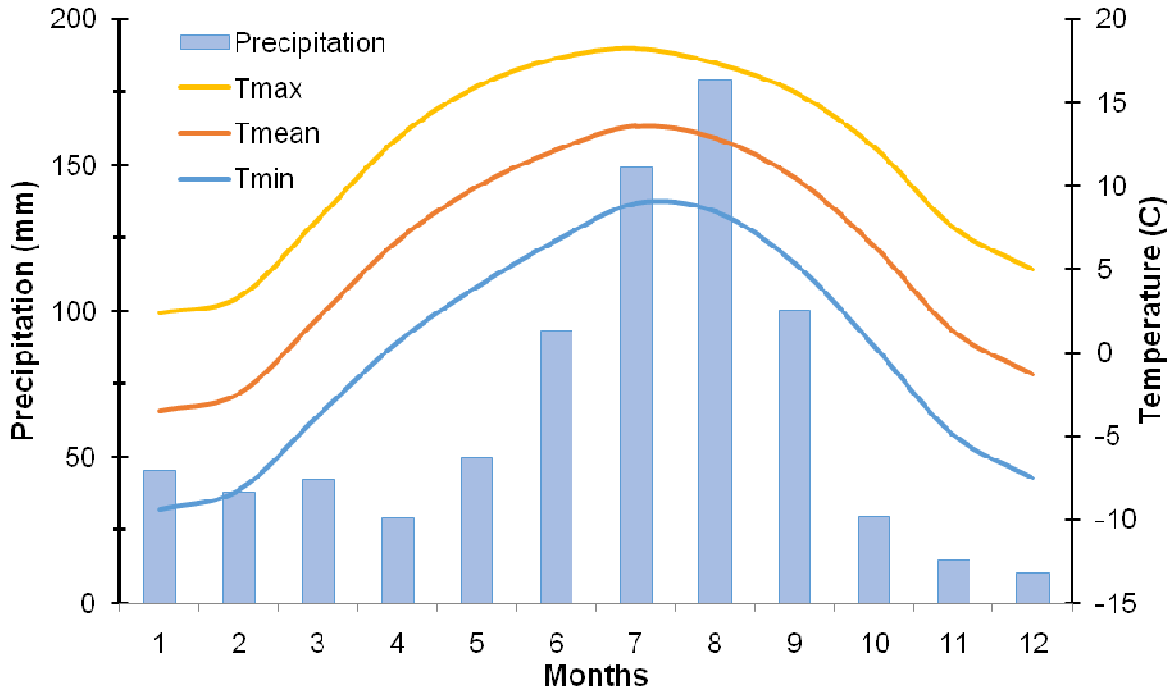

Figure S1. **Regional climatology**. Annual mean meteorological condition in our study region (29º 38' to 32º 13' N and 77º 13' to 80º 50' E) as derived from reanalysis dataset (CRU-TS 4.04, 1901-2019; scale: 2.5º).

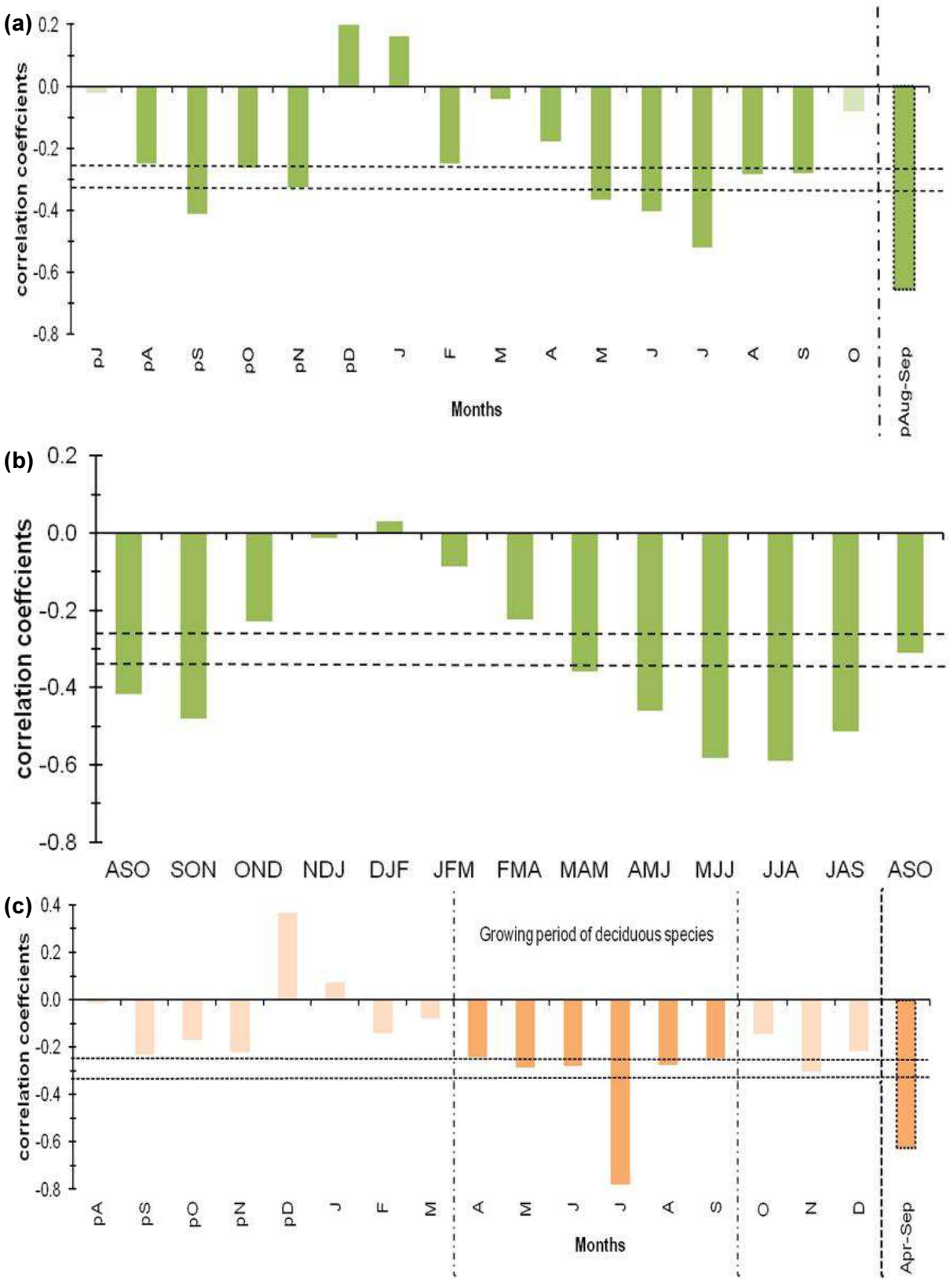
(a)
correlation coeffcients
0.2
0.0
-0.2
-0.4
-0.6
-0.8
pJ
pA
pS
pO
pN
pD
J
F
M
A
M
J
J
A
S
O
pAug-Sep
Months
(b)
correlation coeffcients
0.2
0.0
-0.2
-0.4
-0.6
-0.8
ASO
SON
OND
NDJ
DJF
JFM
FMA
MAM
AMJ
MJJ
JJA
JAS
ASO
(c)
correlation coeffcients
0.4
0.2
0.0
-0.2
-0.4
-0.6
-0.8
Growing period of deciduous species
pA
pS
pO
pN
pD
J
F
M
A
M
J
J
A
S
O
N
D
Apr-Sep
Months

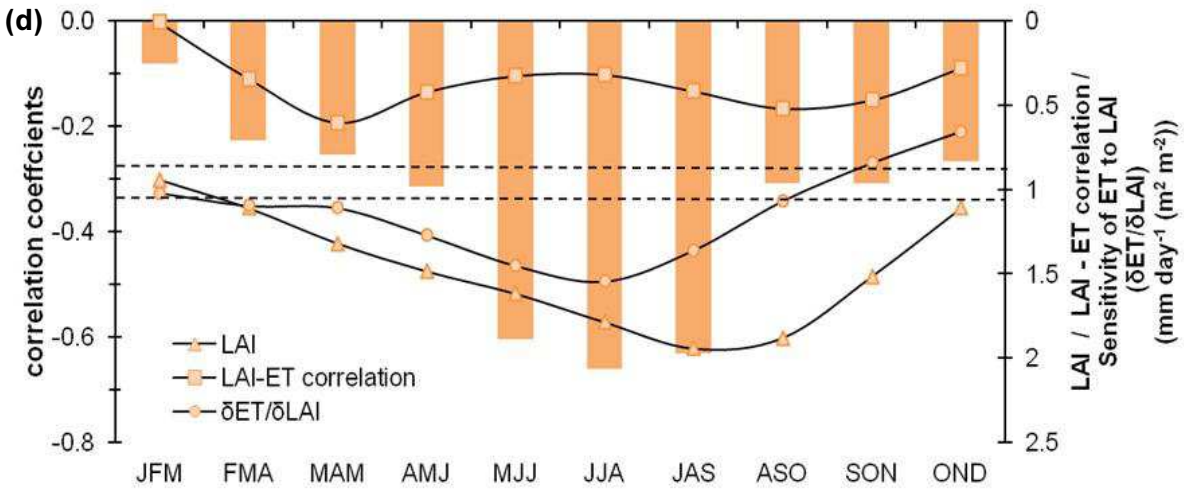

Figure S2. **Hydroclimate-response function**. (a) Monthly correlations between regional conifer $\delta^{18}O$ chronologies with atmospheric moisture content (AMC), (b) Three-month moving correlation coefficients between regional conifer $\delta^{18}O$ chronologies and AMC, (c) Monthly correlations between broadleaf deciduous $\delta^{18}O$ chronology with AMC, and (d) Three-month moving correlation coefficients between broadleaf deciduous $\delta^{18}O$ chronology with AMC. It has been shown with three-month moving average of leaf area index (LAI), correlation between evapotranspiration (ET) and LAI, and the sensitivity of ET to LAI ($\Delta ET/\Delta LAI$: mm day^{-1} (m^2 m^{-2})). The dotted horizontal lines indicate the 95 % and 99 % confidence level respectively. Prefix '*p*' before the months denotes the months of the previous growth year.

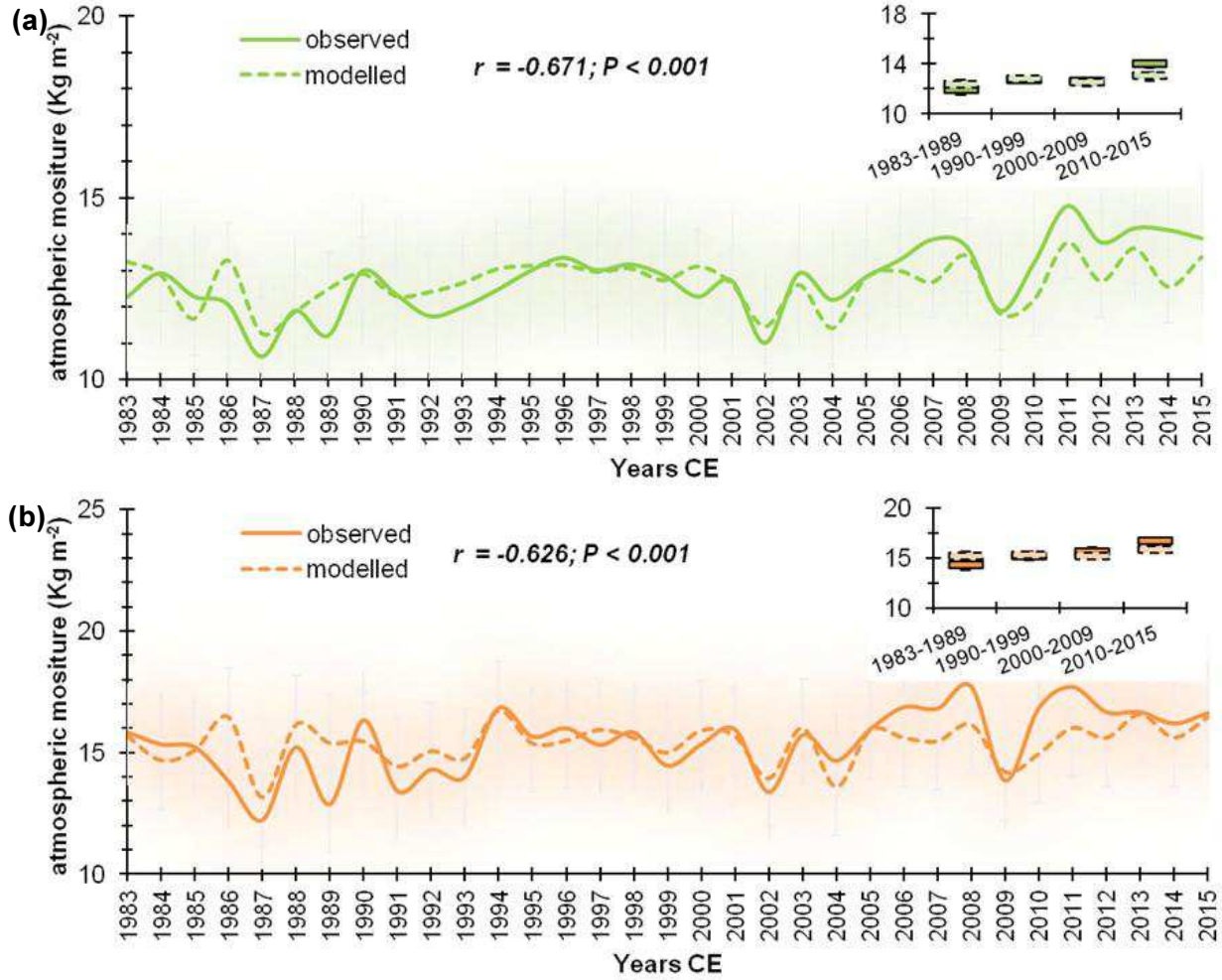

Figure S3. Comparison plot of observed and reconstructed AMC. (a) with regional conifer $\delta^{18}O$ chronologies, and (b) with broadleaf deciduous $\delta^{18}O$ chronology. Inset plot indicates long-term coherence, while shades denote 95 % prediction limit.

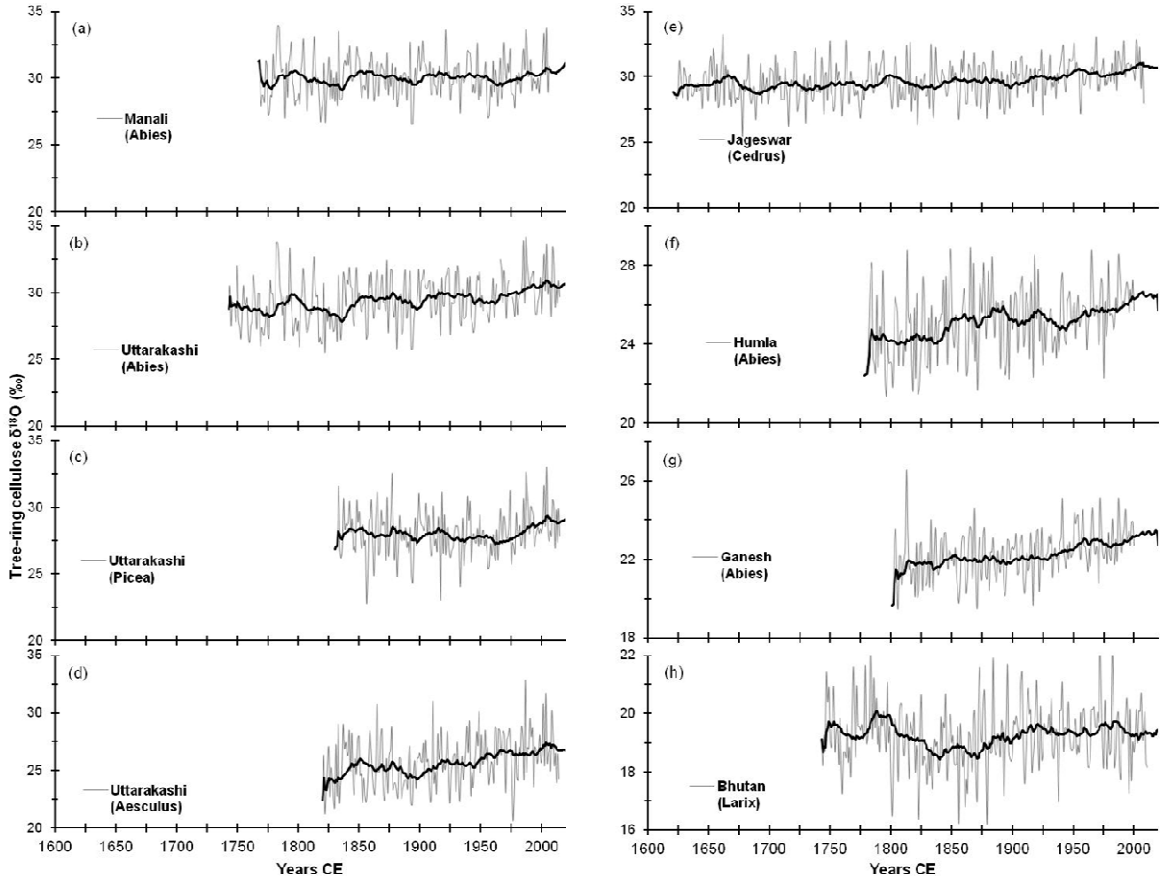

Figure S4. Tree-ring oxygen isotope chronologies of diverse plant functional types from six sites across the central Himalaya. (a) *Abies pindrow* (Manali: Sano et al., 2017), (b-d) *Abies pindrow*, *Picea smithiana*, and *Aesculus indica* (Uttarakashi: Singh et al., 2019), (e) *Cedrus deodara* (Jageshwar: Xu et al., 2018), (f) *Abies spectabilis* (Humla: Sano et al., 2012), (g) *Abies spectabilis* (Ganesh: Xu et al., 2018), and (h) *Larix griffithii* (Bhutan: Sano et al., 2013). Black lines in the site chronologies denote 21 year moving average.

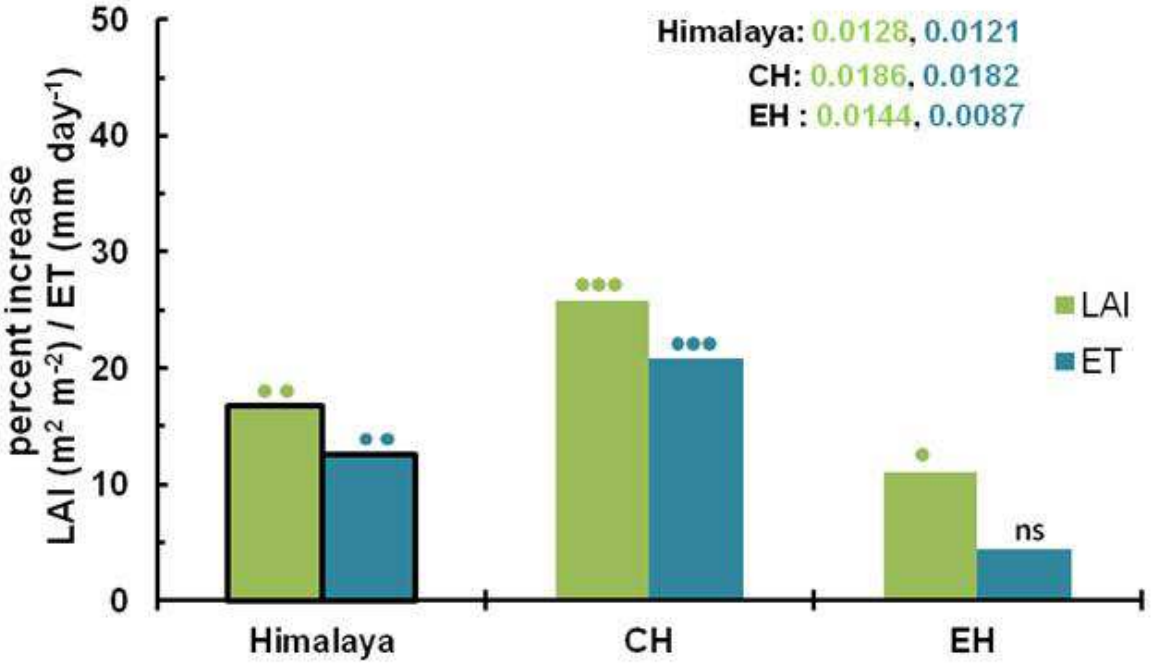

Figure S5. MODIS LAI and ET product since 2000 CE indicates that both LAI and ET in the Himalaya have increased by 16.7% and 12.5% respectively (**$P < 0.05$). Among its regions, greatest increase in ET as well as LAI has been observed for the central Himalaya (CH) (***$P < 0.001$); while for the eastern Himalaya (EH) increase is minimal and non-significant (*$P > 0.05$; $^{ns}P > 0.1$). Sen's slope for ET and LAI has been indicated as inset.

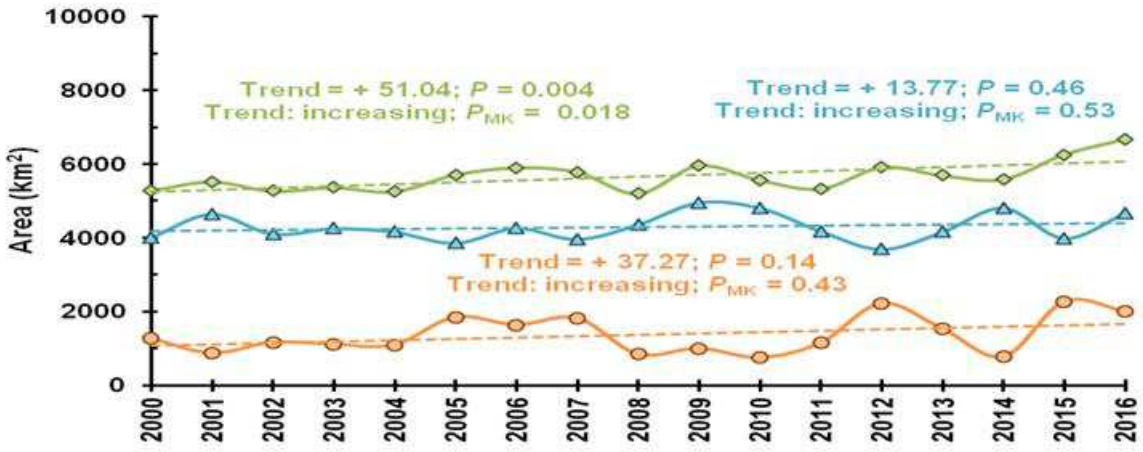

Figure S6. MODIS derived (resolution: 250 m; NDVI > 0.3) regional vegetation trend. Green lines indicates trend during summer when both conifer and deciduous species are green. Faded blue lines denote vegetation trend during winter when only conifers are green. Orange lines indicate trends in deciduous vegetation (as difference between summer and winter-time vegetation).

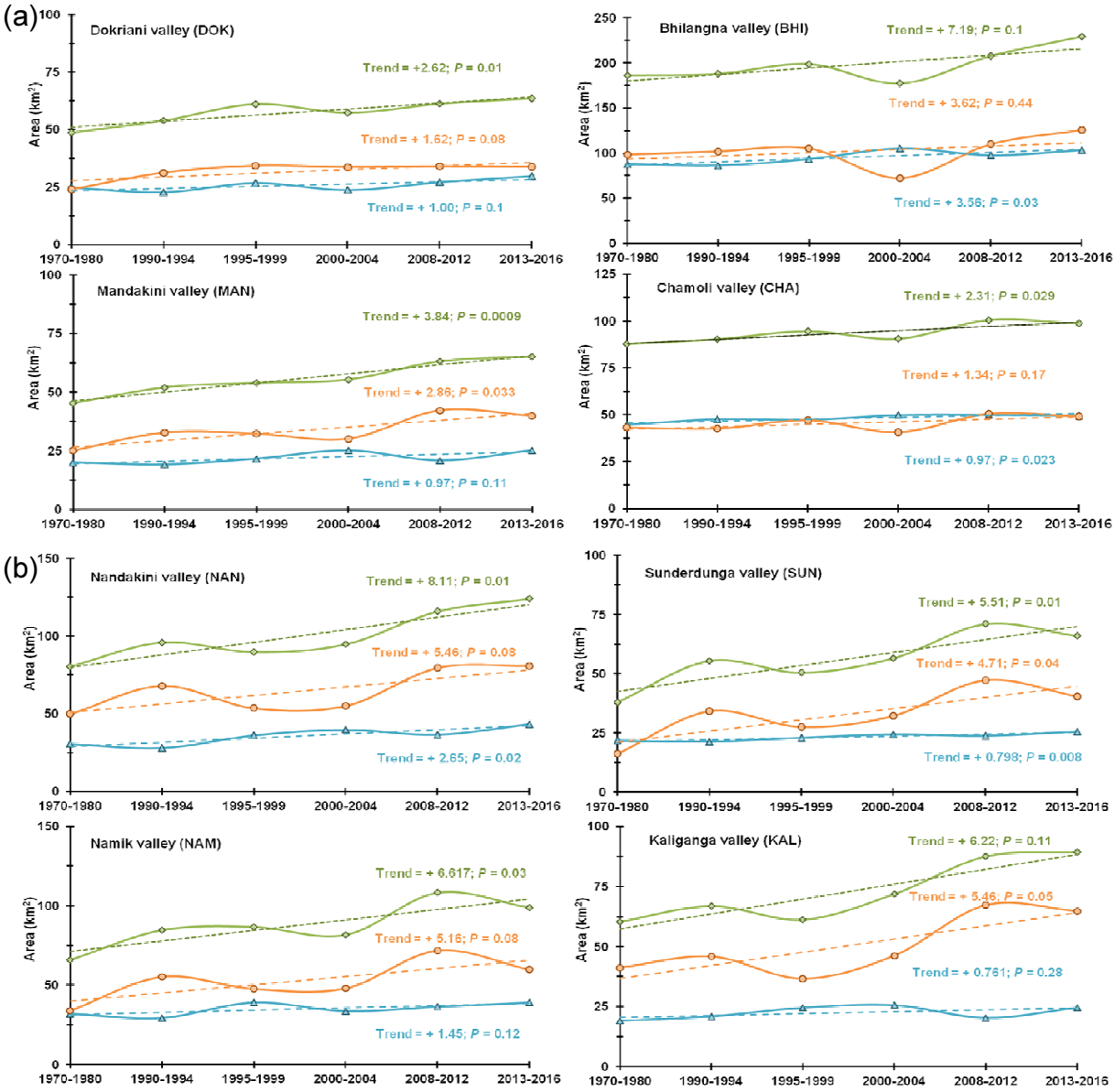

Figure S7. (**a, b**) Landsat (resolution: 30 m) derived glacier valley-scale vegetation trends since 1970s (table S2). Green lines indicates trend during summer when both conifer and deciduous species are green. Faded blue lines denote vegetation trend during winter when only conifers are green. Orange lines indicate trends in deciduous vegetation (as difference between summer and winter-time vegetation). The rate of increase in deciduous vegetation relative to evergreen conifers (winter-time vegetation) is considerably high.

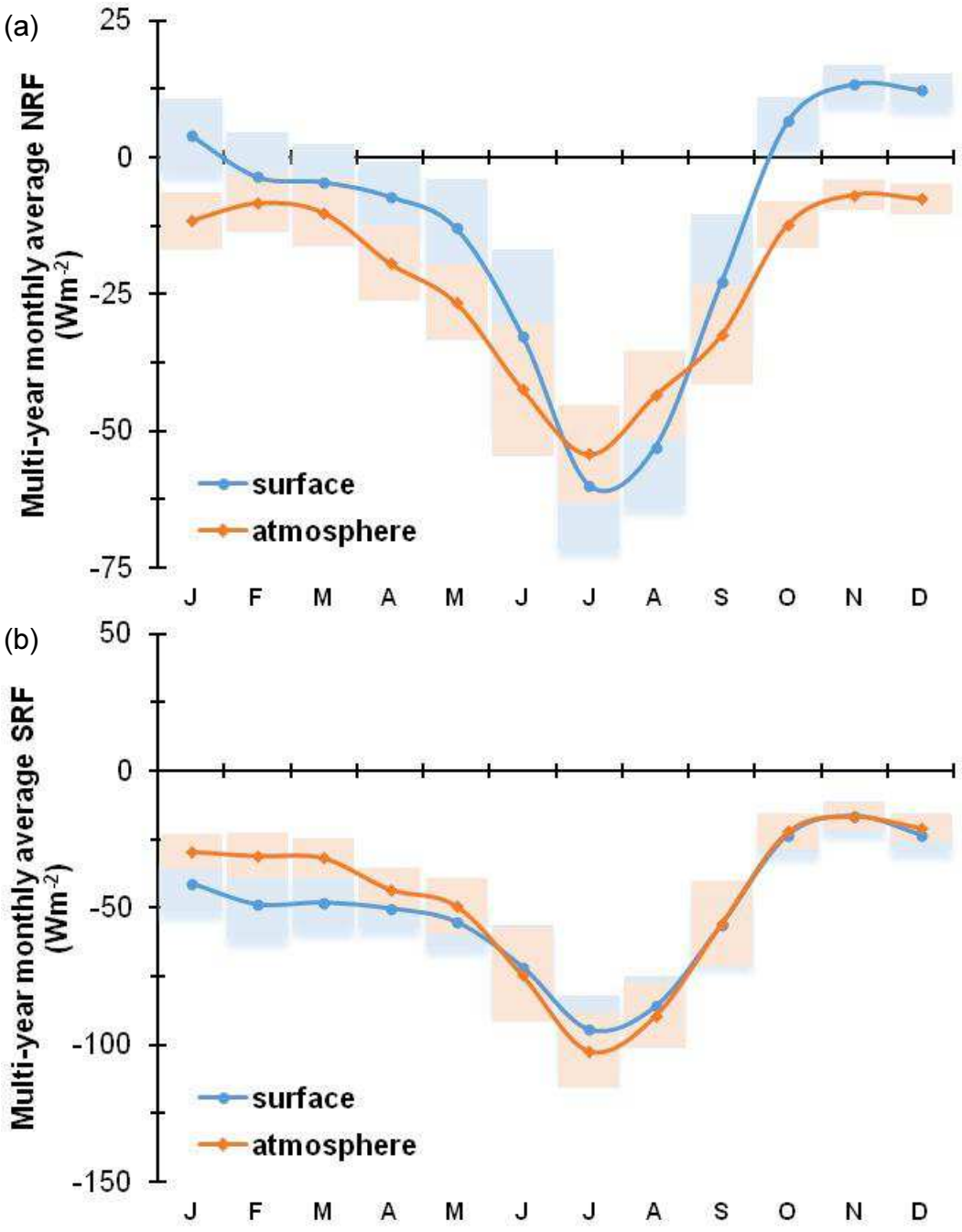
(a)
Multi-year monthly average NRF (Wm-2)
25
0
-25
-50
-75
surface
atmosphere
J F M A M J J A S O N D
(b)
Multi-year monthly average SRF (Wm-2)
50
0
-50
-100
-150
surface
atmosphere
J F M A M J J A S O N D

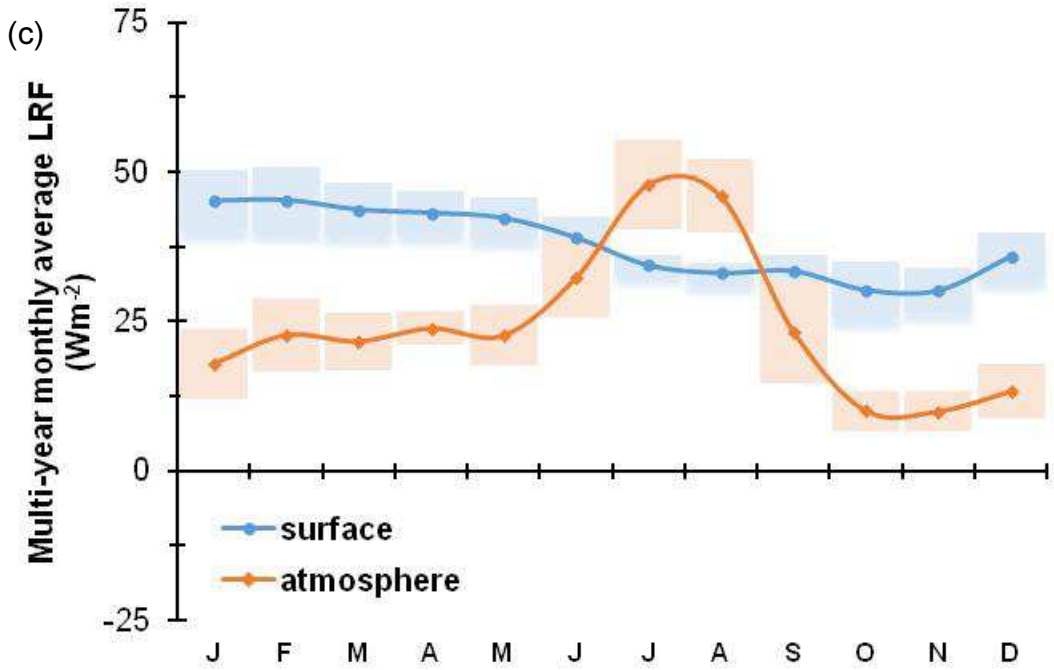

Figure S8. CERES radiation dataset (2000 - 2018) covering glacier valleys in the WCH region showing (a) net radiative forcing (NRF) both at surface and atmosphere, (b) shortwave (SRF), and (c) longwave (LRF).

Supplementary Tables:

Table S1. Details of the satellite dataset utilized in this study.

Sl. No.	Name of data set/ satellite/sensor	Years	Band	Resolution		Swath width	Data downloaded/ processed
				Spatial	Temporal		
1	Landsat MSS	1972-1980	4	68 m x 83 m	18 days	185 km x 185 km	124
2	Landsat TM	1989-2011	7	30 m	16 days	183 km x 172 km	412
3	Landsat 7 ETM+	1999-2003	8	30 m	16 days	183 km x 170 km	102
4	Landsat 8 OLI	2013-2016	11	30 m	16 days	183 km x 170 km	128
5	Terra/MODIS	2000-2016	36	250 m	1-2 days	2330 km	384
6	MODIS: LAI: MOD15A2H and ET: MOD16A2	2000-2018	--	500 m	8-day composite	--	327

Table S2. Geographical statistics of eight glacier valleys in the study region

Sl. No.	Valley	Glacier	Latitude	Longitude	Area (km^2) / Perimeter (km)	Elevation (Min / Max) (m)
1	Dokriani (DOK)	Dokriani	30°48'20.99" 30°53'38.56"	78°39'31.17" 78°51'10.22"	88 / 52	~2000 / 6387
2	Bhilangana (BHI)		30°33'0.52" 30°52'43.37"	78°46'53.54" 79°2'6.18"	418 / 117	~2000 / 6728
3	Mandakini (MAN)	Chorabari	30°36'23.92" 30°44'16.74"	79°8'33.12" 79°19'26.28"	123 / 59	~2000 / 6951
4	Chamoli (CHA)	Tipra Bamak	30°27'53.79" 30°39'7.36"	79°17'40.56" 79°24'56.88"	132 / 60	~2000 / 5844
5	Nandakini (NAN)	Dunagiri	30°13'51.3" 30°20'57.61"	79°34'12.97" 79°46'28.31"	165 / 63	~2000 / 6798
6	Sunderdunga (SUN)		30°6'49.21" 30°17'58.38"	79°47'55" 79°57'42.35"	184 / 68	~2000 / 6850
7	Namik (NAM)		30°4'30.97" 30°14'6.39"	80°2'2.99" 80°9'47.17"	131 / 54	~2000 / 6030
8	Kaliganga (KAL)		30°4'58.95" 30°15'9.72"	80°18'12.37" 80°28'17.28"	167 / 62	~2000 / 6863
9	Above eight valleys		29°54'0.49" 31°0'36.03"	78°30'44.97" 80°31'6.1"	8145 / 472	~1000 / 7811

Table S3. Statistics of calibration, and leave-one-out cross-validation (LOOCV) for April - September, and annual (pAugust - September) AMC reconstructions

Statistics of Calibration (time span: 1982/1983 - 2014/2015 C.E.)

	r	R^2	Adjusted R-squared	F-test	RSE	RMSE	AIC	BIC	DW
April-Sept AMC	-0.626**	0.392	0.372	20.01**	1.077	0.960	102.4	106.9	1.584*
Annual AMC	-0.671**	0.450	0.432	25.41**	0.715	0.637	75.47	79.96	1.242**

[* $p < 0.05$, **$P < 0.001$]

Leave-one-out cross-validation (LOOCV)

	r	R^2	MAE	RMSE	ST (+/-)	PMT	RE	CE	DW
April-Sept AMC	-0.559**	0.313	0.878	1.112	27*+ / 6*−	1.394	0.299	0.450	1.405**
Annual AMC	-0.616**	0.380	0.604	0.737	26*+ / 7*−	2.202	0.459	0.298	1.191*

[* $p < 0.05$, **$P < 0.001$]

r: correlation coefficient; R2: Coefficient of determination (R-squared) or variance explained; F: F-test, RSE: Residual standard error, MAE: Mean Absolute Error, RMSE: Root Mean Square Error, AIC: The Akaike information criterion , BIC: Bayesian information criterion, DW: The Durbin Watson , statistic ST: Sign-test sign, RE: reduction of error; CE: Coefficient of efficiency; PMT: Product mean test, *$p < 0.05$, **$p < 0.001$.